ACS APPLIED MATERIALS & INTERFACES

www.acsami.org

Research Article

Effect of Polysulfide Speciation on Mg Anode Passivation in Mg−S Batteries

Michelle D. Qian, Forrest A. L. Laskowski, Skyler D. Ware, and Kimberly A. See*

Cite This: https://doi.org/10.1021/acsami.2c19488

Read Online

ACCESS | Metrics & More | Article Recommendations | Supporting Information

ABSTRACT: Mg−S batteries are a promising next-generation system for beyond conventional Li-ion chemistry. The Mg−S architecture pairs a Mg metal anode with an inexpensive, high-capacity S_8 cathode. However, S_8-based cathodes exhibit the "polysulfide shuttle" effect, wherein soluble partially reduced S_x^{2-} species generated at the cathode diffuse to and react with the anode. While dissolved polysulfides may undergo reactions to form Li^+-permeable layers in Li−S systems, the interfaces on Mg anodes are passivating. In this work, we probe the reactivity of various Mg polysulfide solutions at the Mg anode interface. Mg polysulfide solutions are prepared without any chelating agents to closely mimic conditions in a Mg−S cell. The polysulfides are synthesized by reacting Mg metal and S_8 in electrolyte, and the speciation is controlled by varying the Mg:S precursor ratio. S-poor precursor ratios produce magnesium polysulfide solutions with a higher proportion of short-chain polysulfides that react at the Mg anode faster than the longer-chain analogues. Anode passivation can be slowed by shifting the polysulfide equilibria toward longer-chain polysulfides through addition of S_8.

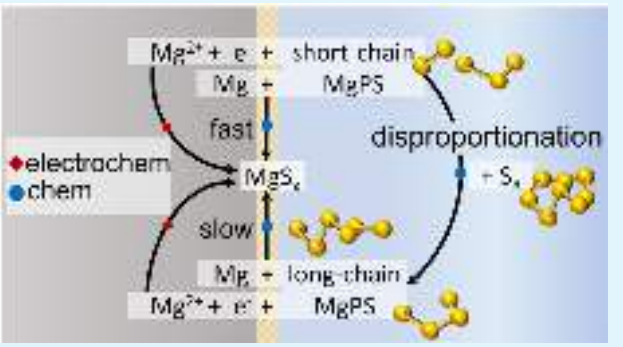

KEYWORDS: *Mg passivation, magnesium polysulfides, Mg−S battery, Mg corrosion, Mg interfaces, polysulfide shuttle*

INTRODUCTION

Li-ion batteries currently dominate the market for both rechargeable portable devices and electric vehicles.[1−4] However, the capacity and cost of the Li-ion batteries are insufficient for long-range transportation and widespread grid-scale energy storage.[3,5,6] Magnesium metal anodes boast capacities higher than the commonly used graphite anode in Li-ion batteries with gravimetric capacities of 2205 vs 372 mAh g^{-1} for graphite and volumetric capacities of 3833 vs 719 mAh cm^{-3} for graphite.[1,2,7,8] Li metal is another option for next-generation anodes; however, dendrite formation risks electrolyte ignition.[9−11] In contrast, Mg forms smoother electrodeposits than Li at the same current densities.[12,13]

The Mg−S battery is a promising architecture that integrates a Mg metal anode with an Earth-abundant elemental sulfur, S_8, cathode. S_8 is environmentally benign, widely abundant,[2−4,14−16] and has a theoretical gravimetric capacity of 1675 mAh g^{-1} assuming full reduction to the metal sulfide—almost an order of magnitude higher than contemporary Li-ion battery cathodes.[3,4,16] Still, identifying an electrolyte simultaneously compatible with both electrodes remains a challenging problem in the Mg−S field. In the past few decades, several electrolytes enabling reversible Mg plating and stripping have been reported; however, Mg−S systems have additional complicating factors. Charge and discharge of the S_8 cathode involve the formation of soluble, partially reduced S_x^{2-} intermediates. S_x^{2-} anions, i.e., polysulfides, can migrate and diffuse to the anode and chemically react to become further reduced, decreasing the reversible capacity and viability of both Mg−S and Li−S batteries.[17−23] Active material loss is also an issue in the analogous Li−S system, but lithium polysulfides in concert with other electrolyte additives can form beneficial solid-electrolyte interphases at the Li anode.[24−26] In contrast, magnesium polysulfides (MgPS) passivate the Mg anode in Mg−S systems, thereby increasing stripping and plating overpotentials.[27,28] The reaction of dissolved polysulfide species with Mg metal is suggested to form very stable surface layers containing MgS that passivate the surface.[29] The fast reactivity of dissolved polysulfide species at the Mg anode causes worsened self-discharge in Mg−S cells compared to Li−S cells.[30]

Understanding Mg anode passivation in Mg−S systems is nontrivial because polysulfides generally exhibit complex dissociation equilibria. Bieker et al. conducted the first study of chemically synthesized polysulfides in solvents relevant for

Received: October 29, 2022
Accepted: January 30, 2023

Mg−S batteries.[28] They proposed the following generally accepted equations as governing Mg polysulfide speciation and equilibria:[28]

$$4S_8^{2-} \rightleftharpoons 4S_6^{2-} + S_8 \quad (1)$$

$$2S_8^{2-} \rightleftharpoons 2S_4^{2-} + S_8 \quad (2)$$

$$4S_6^{2-} \rightleftharpoons 4S_4^{2-} + S_8 \quad (3)$$

$$2S_6^{2-} \rightleftharpoons S_4^{2-} + S_8^{2-} \quad (4)$$

$$S_8^{2-} \rightleftharpoons 2S_4^{\bullet-} \quad (5)$$

$$S_6^{2-} \rightleftharpoons 2S_3^{\bullet-} \quad (6)$$

$$S_4^{2-} \rightleftharpoons 2S_2^{\bullet-} \quad (7)$$

The proposed reactions are in general agreement with the disproportionation reactions suggested by Tobishima et al. for alkali metal polysulfides.[31] The equilibria are interdependent and temperature-, concentration-, and solvent-dependent.[20,28,31−34]

Interestingly, we have shown that the speciation of the polysulfide compounds has a significant effect on the rate of Mg passivation.[27] We recently demonstrated that elemental S_8 dissolved in electrolyte counterintuitively causes lower deposition overpotentials at higher concentrations, suggesting that the reactivity is related to the polysulfide speciation.[27] We hypothesized that lower concentrations of S_8 are more likely to contain shorter-chain polysulfides, and thus, the short-chain polysulfides cause faster passivation of the Mg anode.[27] Higher concentrations of S_8 will favor the left side of eqs 1−3, resulting in the promotion of long-chain polysulfide formation over short-chain polysulfides.

Here, we directly investigate the reactivity of various polysulfide chain lengths at the Mg electrode. MgPS solutions are prepared with varying distributions of polysulfide chain lengths without chelating agents and in conditions relevant to Mg−S cells. The reactivity of the MgPS solutions at the Mg anode is investigated by measuring deposition and stripping overpotentials at the Mg anode vs a Ag_2S quasireference electrode. We show that solutions with short-chain polysulfides cause higher overpotentials earlier in the cycling. Furthermore, we demonstrate that addition of S_8 reduces the overpotentials at the anode due to a shift in the speciation equilibria toward longer-chain polysulfides.

RESULTS AND DISCUSSION

Magnesium Polysulfide Synthesis. To investigate the reactivity of various MgPS molecules at the Mg anode, we must first prepare solutions of MgPS with varying chain lengths. Alkali polysulfides can be synthesized by reacting S_8 directly with reducing metals suspended in solvent.[31,35,36] The reducing metal causes ring-opening reduction reactions to produce polysulfides.[31] Although lithium polysulfides can be produced using either lithium metal or Li_2S as the reducing agent,[9,20,28,31,37] Mg polysulfide synthesis is rare in the literature. Mg polysulfides have been synthesized with a chelating agent *N*-methylimidazole that helps solubilize Mg^{2+} in solution.[9,28,38] However, solutions made with chelating agents may not accurately reflect polysulfide speciation in an electrochemical cell.

Therefore, we aim to prepare MgPS without the use of a chelating agent to more accurately reflect the compounds that would be formed as intermediates in a Mg−S cell. A few examples of preparations without chelators can be found in the literature. Ford et al. synthesized polysulfides directly from Mg and S_8 powders in dimethoxyethane (DME) with 0.25 M $MgTFSI_2$ + 0.5 M $MgCl_2$ and suggested that the synthesis required the presence of magnesium salts. S_8 reduction to polysulfides was confirmed by UV−vis.[39] Similarly, a MgS_x catholyte was prepared by reacting stoichiometric quantities of S_8 and MgS in tetraethylene glycol dimethyl ether with $Mg(HMDS)_2$, $AlCl_3$, and $MgCl_2$.[40] One example of MgPS synthesis in neat solvent was reported by Zhao-Karger et al. in which Mg metal and S_8 powders were reacted in diglyme; however, no characterization of the polysulfides was shown.[41]

The Mg salts in the solution likely activate the Mg metal surface and facilitate reactivity.[39] Thus, we explored the synthesis of MgPS directly in the magnesium aluminum chloride complex (MACC) electrolyte.[42] MACC is a good candidate electrolyte for the present study, as it is prepared by a combination of the simple binary salts $MgCl_2$ and $AlCl_3$ and is non-nucleophilic.[43,44] The MACC electrolyte has been shown to support reversible Mg plating and stripping at low overpotentials after electrochemical conditioning.[42,45] The electrolyte in this study is composed of 30 mM $AlCl_3$ and 60 mM $MgCl_2$ in tetrahydrofuran (THF) and includes 10 mM of the chemical conditioning agent magnesium bis(hexamethyldisilazide) ($Mg(HMDS)_2$). The $Mg(HMDS)_2$ scavenges trace water and promotes formation of free chloride to activate the electrolyte.[46,47] The electrolyte will be referred to simply as MACC−$Mg(HMDS)_2$ hereafter.

Mg polysulfides are synthesized by stirring Mg metal strips with S_8 powder in the MACC−$Mg(HMDS)_2$ electrolyte at 40 °C under Ar for 7 days until a color change is observed. The ratio of Mg:S_8 is varied from a mole ratio of 1:2 Mg:S to 2:1 Mg:S to affect the resulting distribution of polysulfide chain lengths. The speciation is characterized with UV−vis spectroscopy (*vide infra*). S_8-rich conditions (Mg:S 1:2) yield longer-chain polysulfides and are thus called l-MgPS solutions, and S_8-poor conditions (Mg:S 2:1) yield shorter-chain polysulfides and are thus called s-MgPS. All polysulfide syntheses use S_8 in a 62.4 mM concentration of S. Previous direct syntheses of Mg polysulfides have utilized Mg powder,[39,40,48] but attempts to synthesize Mg polysulfides with Mg powder in this system produce inconsistent results, and previous studies cite the passivation of Mg powder as a primary obstacle in a Mg powder synthesis.[28] Attempts to synthesize Mg polysulfides in pure THF without the electrolyte salts, in electrochemically conditioned MACC, or from MgS and S precursors were also unsuccessful. The free Cl^- generated by $Mg(HMDS)_2$ in combination with MACC has been hypothesized to activate Mg metal surfaces to promote facile Mg stripping and deposition,[46,47] and the same activation may be responsible for promoting the formation of Mg polysulfides.

Dissolved polysulfides are difficult to characterize, as they can both disproportionate and oxidize.[14,49] Many literature studies have relied on UV−vis spectroscopy to characterize polysulfides.[9,28,31,50,51] To characterize the MgPS solutions, the solutions are diluted with the MACC−$Mg(HMDS)_2$ electrolyte and analyzed using UV−vis spectroscopy. The absorbance of the Cary 500 used for analyses saturates at roughly 125 mM S, and samples were diluted to accommodate this limit.

https://doi.org/10.1021/acsami.2c19488
ACS Appl. Mater. Interfaces XXXX, XXX, XXX−XXX

Because dilutions will also affect the speciation, discussions of UV−vis data are limited to qualitative and relative descriptions.

UV−vis spectra for S_8, l-MgPS, and s-MgPS solutions in the MACC−$Mg(HMDS)_2$ electrolyte are shown in Figure 1 (an

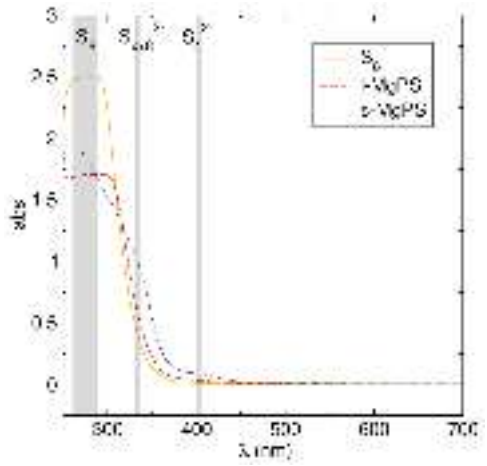

Figure 1. UV−vis spectra of S_8, l-MgPS, and s-MgPS solutions in the MACC−$Mg(HMDS)_2$ electrolyte. The data are shown with the electrolyte spectrum subtracted. The S_8 solution absorbs primarily 260−280 nm, while l-MgPS and s-MgPS both show shoulders in the 335 nm region, with the shoulder in s-MgPS being much more prominent. Both l-MgPS and s-MgPS also show some absorption at 400 nm, again with s-MgPS displaying a higher absorbance. Thus, the l-MgPS solution is composed of more long-chain polysulfides compared to the s-MgPS, which has more short chains.

alternate representation of this data as difference curves with respect to S_8 can be found in Figure S1 in the Supporting Information). Several polysulfide species have more than one absorption peak, and many of the absorption peaks overlap with other species. Disproportionation reactions preclude the isolation of any single polysulfide species for use as a standard.[52,53] Despite the difficulty in assigning exact species, qualitative differences in speciation between the solutions can be observed in the UV−vis spectra. Speciation of polysulfides is solvent-dependent,[20,31,34] so we focus on references in solvents with similar properties to THF (donor number = 20.0 kcal mol^{-1}, dielectric constant ϵ = 7.6).[54] THF absorbs below 250 nm,[31] and only absorbances above 250 nm are used to identify species present in solution. Previous studies in a range of solvents including hexane, water, THF, dioxolane with DME, and tetraglyme attributed absorption in the range of 260−280 nm to elemental S_8.[28,31,50,51,55] In glymes, which have similar donor numbers and ϵ to THF, absorption close to 300 nm is assigned to S_6^{2-},[28] while absorption near 335 nm is assigned to either S_6^{2-} or the short-chain polysulfides S_2^{2-} and S_4^{2-}.[28,48,51,56] Here, absorbances observed in the 300 to 350 nm region are attributed to polysulfide species $S_{x<8}^{2-}$. The yellow color of many polysulfide solutions is the result of the S_4^{2-} chromophore,[31] which absorbs close to 400 nm in dimethyl sulfoxide, glymes, and THF.[20,51,55]

The UV−vis spectra reveal the expected speciation trend. The S_8 solution displays prominent absorption corresponding to elemental S_8. The l-MgPS solution shows similar features to the S_8 solution but with greater absorption in the region of long-chain polysulfides, i.e., $S_{x<8}^{2-}$. The s-MgPS solution shows a greater proportion of short-chain polysulfides, with more prominent absorption features corresponding to $S_{x<8}^{2-}$ and S_4^{2-}. Electrochemical experiments are performed to determine the impact of these differences in speciation on Mg plating overpotentials.

Electrochemical Cycling of Polysulfide Solutions. In our previous work, we observed a counterintuitive result in that Mg anodes cycled in electrolytes with high concentrations of S_8 show lower overpotentials for Mg plating and stripping compared to low concentrations of S_8.[27] We proposed that this was due to the speciation of S with higher S_8 concentrations favoring speciation to long-chain MgPS (eqs 1−3) that reduce at the Mg anode slower compared to short-chain MgPS. Thus, here we hypothesize that Mg metal stripping and deposition in l-MgPS will result in slower passivation than in s-MgPS. Chronopotentiometric experiments are used to examine the effect of polysulfide chain length on stripping and plating overpotentials.

We can now directly probe the relative reactivity of different distributions of polysulfides at the Mg anode using the synthesized polysulfide solutions. To evaluate the relative reactivity of the S_8, l-MgPS, and s-MgPS solutions at the Mg anode, we turn to an adaptation of the deposition and stripping protocol we developed previously.[27] Five cycles of alternating oxidative and reductive current are applied for 30 m intervals, followed by a 3 h open circuit voltage (OCV) rest period. We refer to a pair of oxidative and reductive currents as one cycle, with five cycles composing a set. A Ag_2S quasireference electrode is used to decouple anodic vs cathodic overpotentials. Since the Ag_2S quasireference electrodes drift over time, the OCV rest period is used to probe the Mg/Mg^{2+} redox couple for calculating stripping and plating overpotentials. Polysulfide solutions at the same S concentration are cycled at a current density of ±0.1 mA cm^{-2}, where S concentration is defined as the initial concentration of S used in the syntheses.

The ease of Mg plating is measured by the cathodic overpotential; however, the cathodic overpotential is convoluted by many competing reactions at the Mg anode when S is present in solution. Figure 2 summarizes the possible processes at the Mg|electrolyte interface. When the Mg working electrode is negatively polarized, the electrons can participate in a variety of reduction reactions (Figure 2) including the reduction of Mg^{2+} to Mg metal (plating),

$$Mg^{2+} + 2e^- \rightleftharpoons Mg_{(s)} \tag{8}$$

reduction of dissolved elemental sulfur to long-chain polysulfides,

$$S_8 + 2e^- \rightleftharpoons S_8^{2-} \tag{9}$$

reduction of long-chain polysulfides to short-chain polysulfides,

$$aS_x^{2-} + 2(b-a)e^- \rightleftharpoons cS_y^{2-} + (c-b)S_{cy-ax/c-b}^{2-} \tag{10}$$

and reduction of polysulfides to MgS.

$$S_x^{2-} + Mg^{2+} + 2e^- \rightleftharpoons MgS + S_{x-1}^{2-} \tag{11}$$

In addition to the electrochemical reactions, sulfurous species can also be chemically reduced by Mg metal to MgS.

While all of the possible reduction processes may consume electrons, the kinetically dominant reduction process will depend on and set the voltage of the working electrode in a galvanostatic experiment. When an electronically insulating layer is present on the working electrode, the resistance in the Mg|MACC−$Mg(HMDS)_2$ + MgPS|Mg circuit increases and

https://doi.org/10.1021/acsami.2c19488
ACS Appl. Mater. Interfaces XXXX, XXX, XXX−XXX

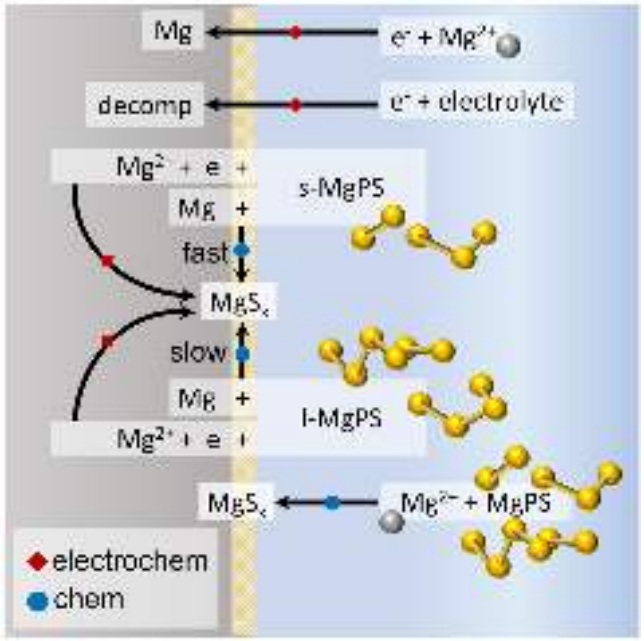

Figure 2. Schematic of the competing reactions at the Mg|MACC−$Mg(HMDS)_2$ + MgPS interface. Electrochemical processes at the interface may include the reduction of Mg^{2+}, MgPS, or the electrolyte. Mg may also react chemically with the polysulfides to form MgS. The reduction of short-chain polysulfides to MgS is proposed to proceed more quickly than reduction of long-chain polysulfides to MgS.

necessitates higher overpotentials to support the same reactions.

First, we discuss the behavior of the neat electrolyte in the cycling experiment with no added S. The voltage curves during cycling for the control cell in neat MACC−$Mg(HMDS)_2$ electrolyte are shown in Figure 3(a). During the first set of cycles, anodic and cathodic potentials are near −1 and −1.5 V vs Ag_2S, respectively. The OCV relaxation period is assumed to approximate the Mg/Mg^{2+} redox couple at −1.3 V vs Ag_2S, and consequently, the overpotentials for stripping and plating observed are less than 300 mV throughout the first set of cycling. Subsequent OCV periods stabilize at −1.4 V vs Ag_2S, and the overpotentials decrease slightly from the initial set to less than 200 mV throughout the remaining 22 h. These results mirror those found for electrochemically conditioned MACC[27] and confirm the previously reported high reversibility of the Mg/Mg^{2+} redox couple in the control MACC−$Mg(HMDS)_2$ system.[46]

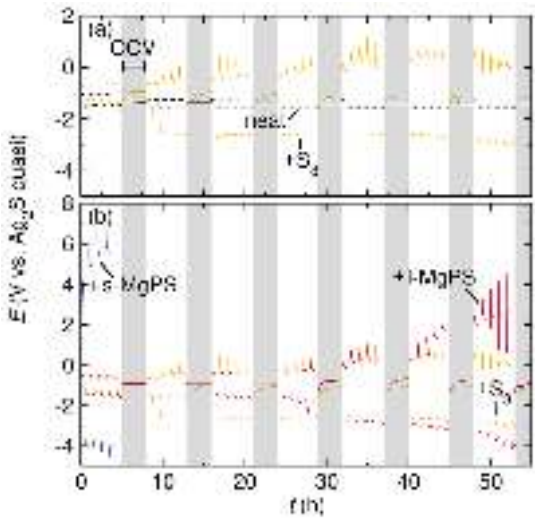

Figure 3. Potential transients measured during the standard cycling experiment of Mg|MACC−$Mg(HMDS)_2$|Mg cells with a Ag_2S quasireference electrode. Electrolyte additives are varied with (a) neat electrolyte and electrolyte with added S_8 and (b) added l-MgPS and added s-MgPS. The results show that the rate of passivation is dependent on the polysulfide solution, with the solutions containing higher proportions of long-chain polysulfides passivating more slowly.

Next, we discuss the effect of adding S_8 to the neat electrolyte. Figure 3(a) shows the potential transients with MACC−$Mg(HMDS)_2$ electrolyte with 62.4 mM S. The cathodic overpotentials eventually reach and stabilize at −2.6 V vs Ag_2S due to the formation of a high-impedance, passivating film on the surface of the Mg that is likely MgS.[27] As soon as the cathodic transients plateau at −2.6 V vs Ag_2S, the anodic overpotentials initially reach very high overpotentials upon polarization but decay over time. The oxidative behavior may be due to the oxidative stripping of the passivating layer that was formed on reduction.[27] These relatively stable anodic overpotentials for a Mg anode are in line with previous studies on Mg stripping and deposition in the presence of S_8.[27,57]

To determine if the speciation of polysulfides changes the passivation layer, the same cycling experiments are performed with l-MgPS and s-MgPS present in the electrolytes. Figure 3(b) shows the potential transients measured in the MACC−$Mg(HMDS)_2$ electrolyte with l-MgPS and s-MgPS. The data measured in the electrolyte + S_8 is replotted for comparison. In the l-MgPS solution, the plating overpotential increases past the voltage measured in the S_8 solution to >−3 V vs Ag_2S. The anodic potentials also jump to greater than 2 V vs Ag_2S (2.5 V overpotential), and the OCV period transient begins to deviate from that of S_8. The high plating and stripping potentials are observed until the end of the 56 h cycling period. The transients measured in the s-MgPS-containing electrolyte show drastically different behavior. The Mg electrode reaches >−3.5 V vs Ag_2S on the first cycle, and the correlated anodic overpotentials are immediately observed. The processes causing polarization are therefore occurring much faster in the s-MgPS solution. The disparate behavior of the Mg electrode in the presence of the three different S-containing solutions suggests that polysulfide speciation is correlated with the rate of Mg anode passivation.

The Mg electrochemistry also depends on the polysulfide concentration. Figure 4 shows the potential transients measured with l-MgPS and s-MgPS electrolytes at 62.4 and 39.9 mM concentrations of S. In both cases, the electrode reaches potentials of >−3 V vs Ag_2S faster with higher polysulfide concentration, suggesting that the reactivity at the interface is dependent on the MgPS concentration. Due to the distinct evolution of the voltage transients that evolve with the 39.9 mM l-MgPS, that electrolyte is selected for extensive characterization on the Mg anode surface. Physical characterization of electrodes cycled in the other solutions can be found in the Supporting Information.

Physical Characterization. To better understand the nature of the passivating layers formed during cycling, characterization methods including scanning electron microscopy (SEM), energy dispersive spectroscopy (EDS), and X-ray photoelectron spectroscopy (XPS) are used. SEM, EDS, and

https://doi.org/10.1021/acsami.2c19488
ACS Appl. Mater. Interfaces XXXX, XXX, XXX−XXX

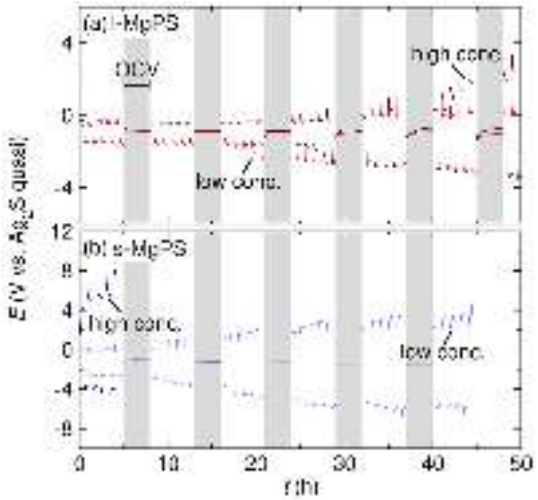

Figure 4. Potential transients measured during the standard cycling experiment for Mg|MACC−$Mg(HMDS)_2$ + MgPS|Mg cells with a Ag_2S reference electrode. Overpotentials are shown for cells with added (a) l-MgPS and (b) s-MgPS. The low-concentration solutions have S concentrations of 39.9 mM, and the high-concentration solutions have S concentrations of 62.4 mM. The lower-concentration polysulfide solutions reach electrolyte decomposition much slower than the higher-concentration polysulfide solutions.

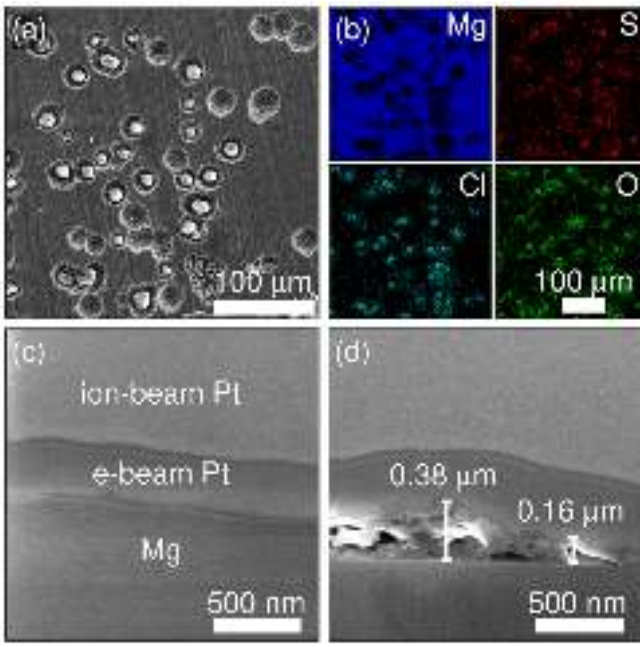

Figure 5. Imaging and spectroscopy of Mg electrodes cycled in electrolyte with l-MgPS until the cathodic overpotential reached −2.65 V vs Ag_2S. (a) SEM shows no surface film although the surface is pitted. (b) EDS maps for Mg, S, Cl, and O show that the Mg distribution is uniform with the exception of the nonconformal circular areas, which correspond to higher concentrations of S, Cl, and O. O is attributed to solvent decomposition and air exposure from transferring the sample into the SEM chamber. (c) HRSEM cross section shows no passivating layer on the Mg surface. (d) HRSEM cross section of a different part of the same electrode shows a new surface layer that is 0.16 to 0.38 μm thick.

XPS of electrodes cycled in neat MACC−$Mg(HMDS)_2$ can be found in the Supporting Information. The surface roughens slightly, and evidence of Cl and O is observed in the EDS. To characterize the surface after exposure to S-containing species, the surfaces of electrodes cycled in solutions with a bulk sulfur concentration of 39.9 mM S for the polysulfide solutions are characterized. For consistency, representative electrodes are characterized immediately following a 30 m cathodic step. Electrodes are rinsed with 1 mL of THF and dried in an Ar-filled glovebox for at least 2 days.

Electrodes from the l-MgPS solutions are selected for SEM analysis. The SEM image and corresponding EDS map of a Mg electrode cycled in l-MgPS until −2.65 V vs Ag_2S are shown in Figure 5(a,b). The SEM reveals a pitted surface with depressions 20−40 μm wide, some of which are filled with a mixture of Cl-, S-, and O-containing particles. No uniform layer is visible on the electrode surface, and the distribution of sulfur is highly variable. The Cl is attributed to electrolyte decomposition. The presence of O is the result of brief air exposure during sample transfer and could also be a product of electrolyte decomposition. To ascertain the presence of a passivating layer, cross sections are milled using a gallium focused ion beam (FIB). Protective platinum is sputtered onto the sample surface prior to milling using an electron beam and ion beam. Figure 5(c,d) shows cross sections from a working electrode using high-resolution SEM (HRSEM). The surface is nonuniformly coated with the porous layer (see Figure S25). The cross section shown in Figure 5(c) was taken from a lighter colored region of the sample when viewed by eye, while the cross section in Figure 5(d) was taken from the grainy, darker layer. Figure 5(c) shows no interfacial layer between the Mg working electrode and protective platinum layers, but Figure 5(d) shows a layer of varying thickness from 0.16 to 0.38 μm.

The Mg electrode can be cycled longer causing even higher overpotentials to be reached. The SEM image and corresponding EDS map for a Mg electrode cycled in l-MgPS polysulfide solution until the cathodic overpotential reaches −4.20 V vs Ag_2S are shown in Figure 6(a,b). The SEM image displays a highly irregular surface with almost no exposed bare Mg metal. S, Cl, and O distribution are more homogeneous than seen for the electrode cycled in l-MgPS until −2.65 V vs Ag_2S (Figure 5). A cross section is milled to determine the thickness of this passivating layer. Figure 6(c,d) shows the SEM images of the cross sections from a working electrode cycled in l-MgPS solution to −4.20 V vs Ag_2S. The surface of this sample is much more irregular than for the electrode cycled to −2.65 V vs Ag_2S, and cross sections were taken from various regions on the electrode. An irregular layer between 0.11 and 0.29 μm thick is observed in Figure 6(c) between the Mg working electrode and protective platinum layers. In Figure 6(d), the layer is much thicker, roughly 3.84 μm. Although the thickness varies, the layer is present across the entire electrode area.

XPS was performed to examine the chemical nature of the passivating layer. We highlight Mg 2p and S 2p regions of the XPS to determine how S is incorporated into the passivating layer (Figure 7). When fitting the Mg 2p region, the spin orbit coupling is ignored because it is very small. For electrodes isolated after cycling to −2.65 V vs Ag_2S, the Mg 2p region of the XPS can be fit with two environments at 48.4 and 50.3 eV (Figure 7(a)). The higher binding energy binding energy environment is is consistent with oxidized Mg, like MgO or MgS.[57−61] The lower binding energy environment is too low to be considered Mg metal. Instead, we assign it to oxidized Mn species.[58,59] Mn is an impurity in the Mg metal that we also detect in X-ray fluorescence analysis of the pristine foil (see

https://doi.org/10.1021/acsami.2c19488
ACS Appl. Mater. Interfaces XXXX, XXX, XXX−XXX

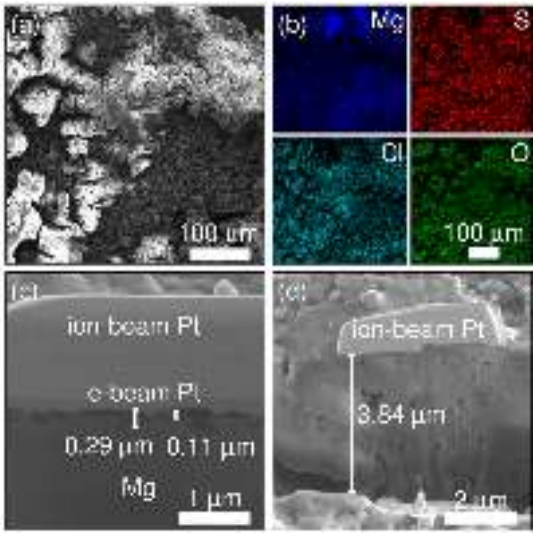

Figure 6. Imaging and spectroscopy of Mg electrodes cycled in electrolyte with l-MgPS until the cathodic overpotential reached −4.20 V vs Ag_2S. (a) SEM shows an insulating, highly nonconformal layer. (b) EDS maps for Mg, S, Cl, and O show less Mg than observed in the electrode cycled until −2.65 V vs Ag_2S. S, Cl, and O are more evenly distributed across the surface than on the electrode cycled until −2.65 V vs Ag_2S. The presence of oxygen is attributed to solvent decomposition and brief air exposure. (c) HRSEM cross section shows the layer thicknesses are between 0.11 to 0.29 μm. (d) HRSEM cross section of a different part of the same electrode shows a layer up to 3.84 μm thick.

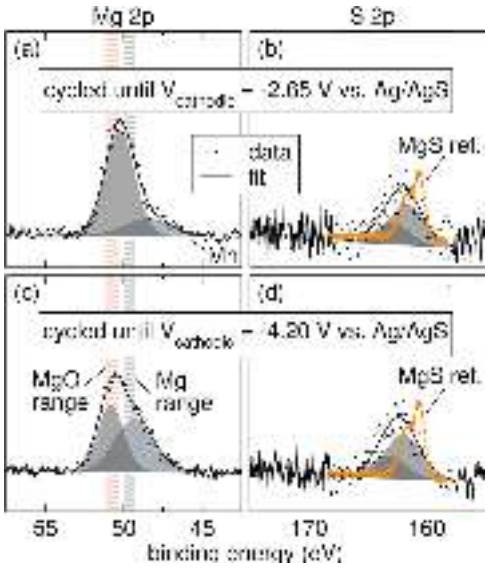

Figure 7. XPS of the Mg 2p and S 2p regions of Mg electrodes cycled until the cathodic overpotentials reached −2.65 V (a,b) and −4.20 V (c,d) vs Ag_2S electrolytes with added l-MgPS. Both electrodes show evidence of oxidized Mg species and MgS_x species.

Figure S32). The S 2p region shows one $2p_{3/2}$ peak at 161.6 eV, negative of the MgS reference spectrum (Figure S31),[65] assigned to MgS_x species.[41,62−64] Based on the layer thickness from HRSEM cross sections, the more reduced MgS may be present beyond the detection depth of XPS. XPS is also measured on a Mg electrode with the thicker passivation layer formed at −4.20 V vs Ag_2S and the results are shown in Figure 7(c,d). Two Mg environments are observed at 49.3 and 50.8 eV. The 49.3 eV peak is broad and assigned to mixed Mn impurity and Mg, while the 50.8 eV peak is assigned to MgO/MgS_x. A S $2p_{3/2}$ peak is observed at 161.9 eV that is assigned to MgS_x.[41,62−64]

The XPS results confirm that the passivating layer includes MgS_x species. In addition, based on the results of EDS analysis, the layer has a significant component of electrolyte decomposition products, corroborating the high overpotentials seen in electrochemical cycling. The Cl and C regions of the XPS do not show any notable differences between the two voltage conditions and thus are shown in the Supporting Information. SEM, EDS, and XPS were also conducted on electrodes cycled in 62.4 mM S in MACC−$Mg(HMDS)_2$ and in s-MgPS and can be found in the Supporting Information. Similar results to l-MgPS were observed for both solutions, although oxidized Mg- and S-containing species near 168 eV are observed on the electrode when S_8 is in solution in addition to MgS_x.

Effects of Sulfur Addition. So far, we have shown that Mg metal electrodes react with S-containing species to form high-impedance surface films. When short-chain polysulfides are present, the film is formed faster. Thus, shifting the equilibrium of S-containing species back to longer-chain polysulfides should slow down passivation. To probe whether the polysulfide equilibria and subsequent passivation can be controlled, S_8 is added to the polysulfide solutions to shift the equilibria. Considering eqs 1−3, we anticipate that addition of S_8 to the polysulfide solutions will push the equilibria to the left and favor long-chain polysulfide populations and thus lower cathodic overpotentials.

To measure how S_8 addition affects the Mg electrodes, S_8 is added at a concentration of 312 mM S during cycling after the passivating layer has developed as indicated by cathodic potentials reaching >−2.6 V vs Ag_2S (Figure 8). S_8 addition to neat electrolyte MACC−$Mg(HMDS)_2$ (black) and electrolyte with added l-MgPS (red) are shown in Figure 8(a). After S_8 is added, the cathodic overpotentials in MACC−$Mg(HMDS)_2$ increase from 200 to 500 mV, while the cathodic overpotentials in the electrolyte with added l-MgPS decrease drastically from 1.9 V to 550 mV. Figure 8(b) shows cycling data for l-MgPS with and without added S_8. At 0 h, both cells have reached cathodic overpotentials of roughly 1.9 V. Slight differences in electrochemical behavior are due to variation in electrode area. With no added S_8, at $t-t_{S_8} > 0$ h, cathodic overpotentials remain near 1.9 V, and anodic overpotentials begin to increase. In the cell with added S_8, at $t-t_{S_8} > 0$ h, cathodic overpotentials are suppressed to 550 mV, and oxidative overpotentials remain constant. These results show that S_8 addition can effectively be used to control polysulfide speciation equilibria and reverse passivation. Based on eqs 1−3, S_8 addition promotes the formation of long-chain polysulfides. Therefore, these findings also support the conclusion that long-chain polysulfides passivate slower than short-chain polysulfides.

CONCLUSIONS

We show that Mg passivation rates are dependent on polysulfide speciation. Polysulfide speciation can be altered in synthesized solutions by varying the input Mg:S ratio, with lower proportions of S correlating to larger proportions of short-chain polysulfides. Short-chain polysulfides are likely preferred because their charge density can be more efficiently

https://doi.org/10.1021/acsami.2c19488
ACS Appl. Mater. Interfaces XXXX, XXX, XXX−XXX

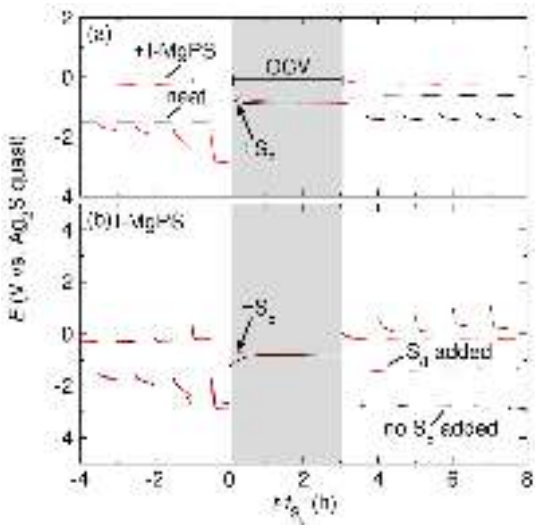

Figure 8. Transient potentials measured from the 4 h before sulfur addition to 8 h after for symmetric Mg cells cycled in neat electrolyte and with l-MgPS. All experimental cells are Mg|MACC−Mg(HMDS)$_2$ (+ polysulfides)|Mg with a Ag_2S quasireference electrode. The *x*-axis ($t-t_{S_8}$) represents the hours of cycling elapsed in relation to the time of sulfur addition. (a) S_8 addition to neat electrolyte results in plating overpotential increases, while S_8 addition to l-MgPS results in overpotential suppresion. (b) Both cells contain added l-MgPS, with one undergoing sulfur addition and the other left as a control. At 0 h, both cells have reached plating overpotentials of roughly 1.9 V. With no added S_8, at $t-t_{S_8} > 0$ h, plating overpotentials remain near 1.9 V. In the cell with added S_8, at $t-t_{S_8} > 0$ h plating overpotentials are suppressed to 550 mV. These results show that plating overpotentials can be controlled via S_8 addition. Full cycling data can be found in the SI.

compensated by divalent Mg^{2+} in a low-dieletric, low-donor solvent like THF. Furthermore, the results show that the initial proportion of polysulfide species impacts subsequent cycling behavior. Rate of overpotential increase is inversely correlated with chain-length of polysulfides in solution—s-MgPS contains the largest population of short-chain polysulfides and experiences rapid overpotential growth. This supports our previous hypothesis that MgS passivation product formation is easier by reaction with short-chain polysulfides than long-chain polysulfides.[27,30] Reduction of short-chain polysulfides to MgS is a less intensive reaction with respect to the number of electrons transferred leading to faster reduction kinetics compared to reduction of longer-chain polysulfides. Through SEM imaging and XPS, the thin passivating layer at overpotentials of 1.6 V is determined to be irregularly deposited MgS_x, MgS, and chlorine-containing electrolyte decomposition species. The thicker passivating layer at overpotentials greater than 2.5 V contains both MgS_x and large quantities of electrolyte decomposition products.

Addition of S_8 shifts polysulfide speciation equilibria toward long-chain polysulfides and thereby suppresses cathodic overpotential growth. Addition of S_8 reduces overpotentials by >1 V when added to an electrolyte with dissolved l-MgPS. Although Mg metal passivation in Mg−S batteries is a recognized problem,[29,30,39] the present study suggests that the passivation rate will be dependent on the S speciation. Overall, these conclusions provide insight into the complexity of polysulfide equilibria and reactions during cycling. The mechanisms for interfacial passivation may inform other next-generation battery designs reliant on charge-dense cations.

EXPERIMENTAL SECTION

Polysulfide Synthesis. The MACC electrolyte was prepared in an Ar-filled glovebox according to Barile et al. with the addition of Mg(HMDS)$_2$ as in Kim et al. in 20 mL batches.[45,46] Tetrahydrofuran (THF, 99.9%, Fisher Scientific) was dried in a Pure Process Technology solvent purification system, and anhydrous $AlCl_3$ (99.999%), $MgCl_2$ (99.9%), and Mg(HMDS)$_2$ (97%) were purchased from Sigma-Aldrich and Fischer Scientific, respectively. Solutions of MACC−Mg(HMDS)$_2$ (30 mM $AlCl_3$ + 60 mM $MgCl_2$ + 10 mM Mg(HMDS)$_2$) were prepared by adding 10 mL of chilled THF (cooled to approximately 0 °C on a Peltier plate) dropwise to anhydrous $AlCl_3$ (80 mg). THF (10 mL) was added to anyhdrous $MgCl_2$ (114.3 mg) and allowed to stir for 1 min. The $AlCl_3$ was completely dissolved in THF to yield a colorless solution. The $AlCl_3$ and $MgCl_2$ solutions were combined, and the resulting solution was stirred at 420 rpm until clear and colorless (≥6 h). The electrolyte was subsequently conditioned by adding Mg(HMDS)$_2$ (69 mg) and allowed to stir until clear.

To synthesize Mg polysulfides, the oxide layer of Mg metal was scraped off using an X-acto blade, and the Mg was cut into small (<1 cm^2) pieces in an Ar-filled glovebox. The Mg pieces (22.8 and 91.0 mg for Mg:S 1:2 and 2:1, respectively) were combined with sulfur powder (60 mg) in a Schlenk tube, and 30 mL of MACC−Mg(HMDS)$_2$ was added. The solution was subsequently heated to 40 °C and stirred under Ar for 7 days until a color change from clear to yellow was observed. The Mg polysulfides were then brought back into the glovebox and centrifuged three times in 5 min cycles, with the Mg polysulfides being carefully decanted into new tubes between each cycle. All polysulfide syntheses used a 62.4 mM concentration of S.

l-MgPS polysulfide experiments utilized two batches of l-MgPS (UV−vis shown in SI). The second batch was more dilute than the first, and the solution was concentrated by slow evaporation to achieve a concentration close to the first batch.

UV−vis Measurements. Solutions were diluted to a nominal concentration of 6.24 mM S for UV−vis measurements unless otherwise noted. UV−vis measurements were measured on a Cary 500 spectrometer in screw cap cuvettes with a 1 cm path length. The MACC−Mg(HMDS)$_2$ in the THF electrolyte spectrum was subtracted as the background.

Ag_2S Quasireference Electrode Preparation. Ag_2S quasireference electrodes were prepared according to literature precedent.[27,66,67] Aqueous $(NH_4)_2S$ (5 wt %) was diluted from a 40−48 wt % stock (Sigma-Aldrich) with deionized (DI) water. The solution was sparged for 30 min with Ar. Ag wires (99.9%, Sigma-Aldrich) were cleaned with 1500 grit silicon carbide paper (McMaster-Carr) and subjected to a single reducing chronoamperometry step at −0.5 V vs a Ag/AgCl reference electrode in 1 M aqueous KCl solution for 2 min to remove surface oxides. The Ag wires were then rinsed with DI water prior to submersion in the $(NH_4)_2S$ solution for 24 h while sparging with Ar.

Electrochemical Testing. All electrochemical cells were prepared in an Ar-filled glovebox. Electrochemical experiments were conducted on a VMP3 potentiostat (Bio-Logic). Three-electrode cells with an Ag_2S quasi-RE and Mg foil (99.9%, MTI) working electrode (WE) and counter electrode (CE) were assembled in 1.8 mL screw-thread borosilicate vials (VWR) with 1.5 mL of electrolyte. WE surface area was measured by taking a photograph of the cell and measuring the submerged area using ImageJ. Cells were cycled at a current density of 0.1 mA cm^{-2}. WE surface area varied between experiments but generally was maintained between 0.4−0.6 cm^2.

Electrochemical Testing with S_8 Addition. All electrochemical cells were prepared in an Ar-filled glovebox. Electrochemical experiments were conducted on a VMP3 potentiostat (Bio-Logic). For initial sulfur addition, S was added at a concentration of 312 mM to 1.5 mL of Mg polysulfides (or 1.5 mL of MACC−Mg(HMDS)$_2$ with S_8 for the elemental sulfur studies), and cycling proceeded as

https://doi.org/10.1021/acsami.2c19488
ACS Appl. Mater. Interfaces XXXX, XXX, XXX−XXX

previously described. For S addition after MgS passivation, three-electrode cells as previously described were cycled until overpotentials reached 1.6 V, at which point the experiment was paused, 10 mg mL^{-1} of S_8 was added, and the cells were reassembled with the same WE, CE, and quasi-RE. For longer experiments, some solvent evaporation was observed over time. THF was added as needed to maintain a total volume of 1.5 mL,and minimal voltage shift (<60 mV) was observed during THF addition. After solvent addition, the cell was then allowed to rest at OCV for 3 h prior to continuation of the experiment. All S addition experiments were run in at least triplicate.

SEM and EDS. All characterization was completed on working electrodes after rinsing with 1 mL of THF and drying in an Ar glovebox for at least 2 days. Samples were briefly exposed to air during transfer into the instrument. SEM images were taken with a ZEISS 1150 VP field emission scanning electron microscope with a 15 kV accelerating voltage and an in-lens secondary electron detector. EDS data were collected using an Oxford X-Max SDD X-ray energy dispersive spectrometer with a 15 kV accelerating voltage.

HRSEM Cross Sections. All characterization was completed on working electrodes after rinsing with 1 mL of THF and drying in an Ar glovebox for at least 2 days. Samples were briefly exposed to air during transfer into the instrument sample holders. Images were taken with a Nova 600 NanoLab equipped with a field emission gun (FEG), scanning electron microscope (SEM), and gallium focused ion beam (Ga-FIB). Prior to milling cross sections, all samples were protected with a layer of electron-beam-deposited platinum and ion-beam-deposited platinum using a gas injection system (GIS).

MgS Synthesis. All materials and precursors were handled inside an Ar-filled glovebox. MgS was prepared by solid-state synthesis similar to Kobayashi et al.[68] Mg (Alfa Aesar, 99.8%) and S (S_8, Acros Organics, >99.5%) powders were ground in stoichiometric quantities and pressed into a pellet of 300 mg with a hand-operated arbor press. The pellet was placed inside a vitreous silica ampule, evacuated to ≤10 mTorr, and sealed with a methane-oxygen torch without exposure to air. The ampule was heated at 2 °C min^{-1} to 600 °C with a dwell time of 24 h. After ambient cooling to room temperature, the ampule was opened inside the glovebox, ground into a fine gray powder, and determined to be phase-pure by X-ray diffraction (XRD). Samples for characterization were mounted on glass slides with polyimide tape to prevent air exposure, and XRD was performed using a Panalytical X'Pert Pro with Cu Kα radiation.

XPS. Each XPS sample was rinsed with 1 mL of THF (Sigma-Aldrich, 99.5%) and dried under ambient glovebox conditions for at least 48 h before analysis. XPS data for l-MgPS were collected using a Surface Science Instruments M-Probe ESCA controlled by Hawk Data Collection software. Low-resolution survey spectra were acquired between binding energies of 1−1000 eV. Higher-resolution detailed scans, with a resolution of 0.08 eV, were collected on individual XPS lines of interest. The sample chamber was maintained at $<2 \times 10^{-8}$ Torr. The XPS data were analyzed using CasaXPS analysis software, and individual peaks of interest were fit with Shirley backgrounds. Peaks were fit using asymmetric Gaussian−Lorentzian line shapes. Adventitious carbon was calibrated to 285 eV. S 2p peaks were fit as doublets with a 1.2 eV splitting.[64] Mg 2p splitting is on the order of 0.28 eV.[69,70] No effect in assignment was seen without taking spin−orbit splitting into account, and Mg 2p peaks were fit as singlets.

X-ray Fluorescence. A Mg foil was manually abladed to remove surface oxides. XRF analysis of the foil was performed with a Micro-XRF Spectrometer (Bruker M4 TORNADO).

■ ASSOCIATED CONTENT

Supporting Information

The Supporting Information is available free of charge at https://pubs.acs.org/doi/10.1021/acsami.2c19488.

UV−vis spectra of as-synthesized solutions and solutions over the course of cycling; chronopotentiometry of as-synthesized solution and as-synthesized solutions with S_8 addition; physical characterization of Mg electrodes cycled in as-synthesized solutions including SEM, EDS, and XPS; XRF of scraped Mg foil (PDF)

■ AUTHOR INFORMATION

Corresponding Author

Kimberly A. See − *Division of Chemistry and Chemical Engineering, California Institute of Technology, Pasadena, California 91125, United States;* orcid.org/0000-0002-0133-9693; Email: ksee@caltech.edu

Authors

Michelle D. Qian − *Division of Chemistry and Chemical Engineering, California Institute of Technology, Pasadena, California 91125, United States;* orcid.org/0000-0002-4815-1014

Forrest A. L. Laskowski − *Division of Chemistry and Chemical Engineering, California Institute of Technology, Pasadena, California 91125, United States;* orcid.org/0000-0001-8909-483X

Skyler D. Ware − *Division of Chemistry and Chemical Engineering, California Institute of Technology, Pasadena, California 91125, United States;* orcid.org/0000-0002-3249-1946

Complete contact information is available at: https://pubs.acs.org/10.1021/acsami.2c19488

Notes

The authors declare no competing financial interest.

■ ACKNOWLEDGMENTS

M.D.Q. acknowledges support from the National Science Foundation Graduate Research Fellowship under Grant No. DGE1745301. F.A.L.L. acknowledges the support of the Arnold and Mabel Beckman Foundation via a 2020 Arnold O. Beckman Postdoctoral Fellowship in Chemical Sciences. K.A.S. acknowledges support from the David and Lucile Packard Foundation. The authors thank Miguel Cabán-Acevedo and the Kavli Nanoscience Institute for HRSEM imaging, Brian Lee for solid-state synthesis, and Jake Evans for assistance with XPS data collection and fitting. XPS data were collected at the Molecular Materials Research Center in the Beckman Institute of the California Institute of Technology. SEM, EDS, and XRF data were collected at the GPS Division Analytical Facility of the California Institute of Technology.

■ REFERENCES

(1) Besenhard, J. O.; Winter, M. Advances in Battery Technology: Rechargeable Magnesium Batteries and Novel Negative-Electrode Materials for Lithium Ion Batteries. *Chem. Phys. Chem.* **2002**, *3*, 155−159.

(2) Kong, L.; Yan, C.; Huang, J.-Q.; Zhao, M.-Q.; Titirici, M.-M.; Xiang, R.; Zhang, Q. A Review of Advanced Energy Materials for Magnesium−Sulfur Batteries. *Energy Environ. Mater.* **2018**, *1*, 100−112.

(3) Manthiram, A.; Fu, Y.; Su, Y.-S. Challenges and Prospects of Lithium−Sulfur Batteries. *Acc. Chem. Res.* **2013**, *46*, 1125−1134.

(4) Zhao-Karger, Z.; Fichtner, M. Magnesium-Sulfur Battery: Its Beginning and Recent Progress. *MRS Commun.* **2017**, *7*, 770−784.

(5) Thackeray, M. M.; Wolverton, C.; Isaacs, E. D. Electrical Energy Storage for Transportation—Approaching the Limits of, and Going beyond, Lithium-Ion Batteries. *Energy Environ. Sci.* **2012**, *5*, 7854.

(6) Bruce, P. G.; Freunberger, S. A.; Hardwick, L. J.; Tarascon, J.-M. Li−O_2 and Li−S Batteries with High Energy Storage. *Nat. Mater.* **2012**, *11*, 19−29.

(7) Obrovac, M. N.; Chevrier, V. L. Alloy Negative Electrodes for Li-Ion Batteries. *Chem. Rev.* **2014**, *114*, 11444−11502.
(8) Nishi, Y. Lithium Ion Secondary Batteries; Past 10 Years and the Future. *J. Power Sources* **2001**, *100*, 101−106.
(9) Bieker, G.; Diddens, D.; Kolek, M.; Borodin, O.; Winter, M.; Bieker, P.; Jalkanen, K. Cation-Dependent Electrochemistry of Polysulfides in Lithium and Magnesium Electrolyte Solutions. *J. Phys. Chem. C* **2018**, *122*, 21770−21783.
(10) Aurbach, D. A Short Review of Failure Mechanisms of Lithium Metal and Lithiated Graphite Anodes in Liquid Electrolyte Solutions. *Solid State Ion.* **2002**, *148*, 405−416.
(11) Bieker, G.; Winter, M.; Bieker, P. Electrochemical in Situ Investigations of SEI and Dendrite Formation on the Lithium Metal Anode. *Phys. Chem. Chem. Phys.* **2015**, *17*, 8670−8679.
(12) Matsui, M. Study on Electrochemically Deposited Mg Metal. *J. Power Sources* **2011**, *196*, 7048−7055.
(13) Hao, F.; Verma, A.; Mukherjee, P. P. Electrodeposition Stability of Metal Electrodes. *Energy Storage Mater.* **2019**, *20*, 1−6.
(14) Jones, J.-P.; Jones, S. C.; Krause, F. C.; Pasalic, J.; Bugga, R. *In Situ* Polysulfide Detection in Lithium Sulfur Cells. *J. Phys. Chem. Lett.* **2018**, *9*, 3751−3755.
(15) Chen, R.; Zhao, T.; Wu, F. From a Historic Review to Horizons beyond: Lithium−Sulphur Batteries Run on the Wheels. *Chem. Commun.* **2015**, *51*, 18−33.
(16) Ji, X.; Nazar, L. F. Advances in Li−S Batteries. *J. Mater. Chem.* **2010**, *20*, 9821.
(17) Yamin, H.; Peled, E. Electrochemistry of a Nonaqueous Lithium/Sulfur Cell. *J. Power Sources* **1983**, *9*, 281−287.
(18) Coleman, J.; Bates, M. The Sulfur Electrode. *Research and Development in Non-Mechanical Electrical Power Sources* **1970**, 289−302.
(19) Mikhaylik, Y. V.; Akridge, J. R. Polysulfide Shuttle Study in the Li/S Battery System. *J. Electrochem. Soc.* **2004**, *151*, A1969.
(20) Rauh, R.; Shuker, F.; Marston, J.; Brummer, S. Formation of Lithium Polysulfides in Aprotic Media. *J. Inorg. Nucl. Chem.* **1977**, *39*, 1761−1766.
(21) Diao, Y.; Xie, K.; Xiong, S.; Hong, X. Shuttle Phenomenon − The Irreversible Oxidation Mechanism of Sulfur Active Material in Li−S Battery. *J. Power Sources* **2013**, *235*, 181−186.
(22) Zhao-Karger, Z.; Zhao, X.; Wang, D.; Diemant, T.; Behm, R. J.; Fichtner, M. Performance Improvement of Magnesium Sulfur Batteries with Modified Non-Nucleophilic Electrolytes. *Adv. Energy Mater.* **2015**, *5*, 1401155.
(23) Li, W.; Cheng, S.; Wang, J.; Qiu, Y.; Zheng, Z.; Lin, H.; Nanda, S.; Ma, Q.; Xu, Y.; Ye, F.; Liu, M.; Zhou, L.; Zhang, Y. Synthesis, Crystal Structure, and Electrochemical Properties of a Simple Magnesium Electrolyte for Magnesium/Sulfur Batteries. *Angew. Chem., Int. Ed.* **2016**, *55*, 6406−6410.
(24) Li, W.; Yao, H.; Yan, K.; Zheng, G.; Liang, Z.; Chiang, Y.-M.; Cui, Y. The Synergetic Effect of Lithium Polysulfide and Lithium Nitrate to Prevent Lithium Dendrite Growth. *Nat. Commun.* **2015**, *6*, 7436.
(25) Xiong, S.; Xie, K.; Diao, Y.; Hong, X. Characterization of the Solid Electrolyte Interphase on Lithium Anode for Preventing the Shuttle Mechanism in Lithium−Sulfur Batteries. *J. Power Sources* **2014**, *246*, 840−845.
(26) Yan, C.; Cheng, X.-B.; Zhao, C.-Z.; Huang, J.-Q.; Yang, S.-T.; Zhang, Q. Lithium Metal Protection through In-Situ Formed Solid Electrolyte Interphase in Lithium-Sulfur Batteries: The Role of Polysulfides on Lithium Anode. *J. Power Sources* **2016**, *327*, 212−220.
(27) Laskowski, F. A. L.; Stradley, S. H.; Qian, M. D.; See, K. A. Mg Anode Passivation Caused by the Reaction of Dissolved Sulfur in Mg−S Batteries. *ACS Appl. Mater. Interfaces* **2021**, *13*, 29461.
(28) Bieker, G.; Wellmann, J.; Kolek, M.; Jalkanen, K.; Winter, M.; Bieker, P. Influence of Cations in Lithium and Magnesium Polysulphide Solutions: Dependence of the Solvent Chemistry. *Phys. Chem. Chem. Phys.* **2017**, *19*, 11152−11162.
(29) Salama, M.; Attias, R.; Hirsch, B.; Yemini, R.; Gofer, Y.; Noked, M.; Aurbach, D. On the feasibility of practical Mg-S batteries: practical limitations associated with metallic magnesium anodes. *ACS Appl. Mater. Interfaces* **2018**, *10*, 36910−36917.
(30) Richter, R.; Häcker, J.; Zhao-Karger, Z.; Danner, T.; Wagner, N.; Fichtner, M.; Friedrich, K. A.; Latz, A. Insights into Self-Discharge of Lithium− and Magnesium−Sulfur Batteries. *ACS Appl. Energy Mater.* **2020**, *3*, 8457−8474.
(31) Tobishima, S.-I.; Yamamoto, H.; Matsuda, M. Study on the Reduction Species of Sulfur by Alkali Metals in Nonaqueous Solvents. *Electrochimic. Acta* **1997**, *42*, 1019−1029.
(32) Dubois, P.; Lelieur, J. P.; Lepoutre, G. Chemical Species in Solutions of Sulfur in Liquid Ammonia. *Inorg. Chem.* **1987**, *26*, 1897−1902.
(33) Giggenbach, W. F. The Blue Supersulphide Ion, S_2^-. *J. Chem. Soc., Dalton Trans.* **1973**, *7*, 729.
(34) MacColl, R.; Windwer, S. Spectroscopy of Sulfur in Ethylenediamine. *J. Phys. Chem.* **1970**, *74*, 1261−1266.
(35) Cleaver, B.; Davies, A. J.; Schiffrin, D. J. Properties of Fused Polysulphides-V. Voltammetric Studies on Sulphur and Polysulphides in Fused KSCN and LiCl-KCl Eutectic. *Electrochim. Acta* **1973**, *18*, 747−760.
(36) Cleaver, B.; Davies, A.; Hames, M. Properties of Fused Polysulphides—I. The Electrical Conductivity of Fused Sodium and Potassium Polysulphides. *Electrochim. Acta* **1973**, *18*, 719−726.
(37) Vijayakumar, M.; Govind, N.; Walter, E.; Burton, S. D.; Shukla, A.; Devaraj, A.; Xiao, J.; Liu, J.; Wang, C.; Karim, A.; Thevuthasan, S. Molecular Structure and Stability of Dissolved Lithium Polysulfide Species. *Phys. Chem. Chem. Phys.* **2014**, *16*, 10923−10932.
(38) Dev, S.; Ramli, E.; Rauchfuss, T. B.; Wilson, S. R. Synthesis and Structure of $[(\text{N-methylimidazole})_6]S_8$ (M = Manganese, Iron, Nickel, Magnesium). Polysulfide Salts Prepared by the Reaction N-methylimidazole + Metal Powder + Sulfur. *Inorg. Chem.* **1991**, *30*, 2514−2519.
(39) Ford, H. O.; Doyle, E. S.; He, P.; Boggess, W. C.; Oliver, A. G.; Wu, T.; Sterbinsky, G. E.; Schaefer, J. L. Self-Discharge of Magnesium−Sulfur Batteries Leads to Active Material Loss and Poor Shelf Life. *Energy Environ. Sci.* **2021**, *14*, 890−899.
(40) Muthuraj, D.; Pandey, M.; Krishna, M.; Ghosh, A.; Sen, R.; Johari, P.; Mitra, S. Magnesium Polysulfide Catholyte (MgSx): Synthesis, Electrochemical and Computational Study for Magnesium-Sulfur Battery Application. *J. Power Sources* **2021**, *486*, 229326.
(41) Zhao-Karger, Z.; Liu, R.; Dai, W.; Li, Z.; Diemant, T.; Vinayan, B. P.; Bonatto Minella, C.; Yu, X.; Manthiram, A.; Behm, R. J.; Ruben, M.; Fichtner, M. Toward Highly Reversible Magnesium−Sulfur Batteries with Efficient and Practical $Mg[B(Hfip)_4]_2$ Electrolyte. *ACS Energy Lett.* **2018**, *3*, 2005−2013.
(42) Doe, R. E.; Han, R.; Hwang, J.; Gmitter, A. J.; Shterenberg, I.; Yoo, H. D.; Pour, N.; Aurbach, D. Novel, Electrolyte Solutions Comprising Fully Inorganic Salts with High Anodic Stability for Rechargeable Magnesium Batteries. *Chem. Commun.* **2014**, *50*, 243−245.
(43) Liu, T.; Shao, Y.; Li, G.; Gu, M.; Hu, J.; Xu, S.; Nie, Z.; Chen, X.; Wang, C.; Liu, J. A Facile Approach Using $MgCl_2$ to Formulate High Performance Mg^{2+} Electrolytes for Rechargeable Mg Batteries. *J. Mater. Chem. A* **2014**, *2*, 3430.
(44) Bevilacqua, S. C.; Pham, K. H.; See, K. A. Effect of the Electrolyte Solvent on Redox Processes in Mg−S Batteries. *Inorg. Chem.* **2019**, *58*, 10472−10482.
(45) Barile, C. J.; Barile, E. C.; Zavadil, K. R.; Nuzzo, R. G.; Gewirth, A. A. Electrolytic Conditioning of a Magnesium Aluminum Chloride Complex for Reversible Magnesium Deposition. *J. Phys. Chem. C* **2014**, *118*, 27623−27630.
(46) Kim, S. S.; Bevilacqua, S. C.; See, K. A. Conditioning-Free Mg Electrolyte by the Minor Addition of $Mg(HMDS)_2$. *ACS Appl. Mater. Interfaces* **2020**, *12*, 5226−5233.
(47) Kim, S. S.; See, K. A. Activating Magnesium Electrolytes through Chemical Generation of Free Chloride and Removal of Trace Water. *ACS Appl. Mater. Interfaces* **2021**, *13*, 671−680.
(48) He, P.; Ford, H. O.; Gonzalez, S.; Rodriguez, S.; Oliver, A. G.; Schaefer, J. L. Stability and Disproportionation of Magnesium

https://doi.org/10.1021/acsami.2c19488
ACS Appl. Mater. Interfaces XXXX, XXX, XXX−XXX

Polysulfides and the Effects on the Mg-Polysulfide Flow Battery. *J. Electrochem. Soc.* **2021**, *168*, 110516.
(49) Argyropoulos, D. S.; Hou, Y.; Ganesaratnam, R.; Harpp, D. N.; Koda, K. Quantitative ^{1}H NMR Analysis of Alkaline Polysulfide Solutions. *Holzforschung* **2005**, *59*, 124−131.
(50) Friedman, H. L.; Kerker, M. Ultraviolet Absorption of Aqueous Sulfur Solutions. *J. Colloid Sci.* **1953**, *8*, 80−85.
(51) Marceau, H.; Kim, C.-S.; Paolella, A.; Ladouceur, S.; Lagacé, M.; Chaker, M.; Vijh, A.; Guerfi, A.; Julien, C. M.; Mauger, A.; Armand, M.; Hovington, P.; Zaghib, K. In Operando Scanning Electron Microscopy and Ultraviolet−Visible Spectroscopy Studies of Lithium/Sulfur Cells Using All Solid-State Polymer Electrolyte. *J. Power Sources* **2016**, *319*, 247−254.
(52) Giggenbach, W. Optical Spectra and Equilibrium Distribution of Polysulfide Ions in Aqueous Solution at 20°. *Inorg. Chem.* **1972**, *11*, 1201−1207.
(53) Cotton, F. A.; Harmon, J. B.; Hedges, R. M. Calculation of the Ground State Electronic Structures and Electronic Spectra of Di- and Trisulfide Radical Anions by the Scattered Wave-SCF-X.Alpha. Method. *J. Am. Chem. Soc.* **1976**, *98*, 1417−1424.
(54) Gutmann, V. Solvent Effects on the Reactivities of Organometallic Compounds. *Coord. Chem. Rev.* **1976**, *18*, 225−255.
(55) He, Q.; Freiberg, A. T. S.; Patel, M. U. M.; Qian, S.; Gasteiger, H. A. *Operando* Identification of Liquid Intermediates in Lithium−Sulfur Batteries via Transmission UV−Vis Spectroscopy. *J. Electrochem. Soc.* **2020**, *167*, 080508.
(56) Barchasz, C.; Molton, F.; Duboc, C.; Leprêtre, J.-C.; Patoux, S.; Alloin, F. Lithium/Sulfur Cell Discharge Mechanism: An Original Approach for Intermediate Species Identification. *Anal. Chem.* **2012**, *84*, 3973−3980.
(57) Gao, T.; Hou, S.; Huynh, K.; Wang, F.; Eidson, N.; Fan, X.; Han, F.; Luo, C.; Mao, M.; Li, X.; Wang, C. Existence of Solid Electrolyte Interphase in Mg Batteries: Mg/S Chemistry as an Example. *ACS Appl. Mater. Interfaces* **2018**, *10*, 14767−14776.
(58) Chourasia, A. R.; Chopra, D. R. Elemental Manganese Studied by X-ray Photoemission Spectroscopy Using Mg and Zr Radiations. *Surf. Sci. Spectra* **1994**, *3*, 74−81.
(59) Aoki, A. X-Ray Photoelectron Spectroscopic Studies on ZnS: MnF_2 Phosphors. *Jpn. J. Appl. Phys.* **1976**, *15*, 305−311.
(60) Karakalos, S.; Siokou, A.; Ladas, S. The Interfacial Properties of $MgCl_2$ Films Grown on a Flat SiO_2/Si Substrate. An XPS and ISS Study. *Appl. Surf. Sci.* **2009**, *255*, 8941−8946.
(61) Ardizzone, S.; Bianchi, C.; Fadoni, M.; Vercelli, B. Magnesium Salts and Oxide: An XPS Overview. *Appl. Surf. Sci.* **1997**, *119*, 253−259.
(62) Xu, Y.; Zhou, G.; Zhao, S.; Li, W.; Shi, F.; Li, J.; Feng, J.; Zhao, Y.; Wu, Y.; Guo, J.; Cui, Y.; Zhang, Y. Improving a Mg/S Battery with YCl_3 Additive and Magnesium Polysulfide. *Adv. Sci.* **2019**, *6*, 1800981.
(63) Fantauzzi, M.; Elsener, B.; Atzei, D.; Rigoldi, A.; Rossi, A. Exploiting XPS for the Identification of Sulfides and Polysulfides. *RSC Adv.* **2015**, *5*, 75953−75963.
(64) Smart, R. S. C.; Skinner, W. M.; Gerson, A. R. XPS of Sulphide Mineral Surfaces: Metal-deficient, Polysulphides, Defects and Elemental Sulphur. *Surf. Interface Anal.* **1999**, *28*, 101−105.
(65) Franzen, H. F.; Umaña, M. X.; McCreary, J.; Thorn, R. XPS Spectra of Some Transition Metal and Alkaline Earth Monochalcogenides. *J. Solid State Chem.* **1976**, *18*, 363−368.
(66) Dugas, R.; Forero-Saboya, J. D.; Ponrouch, A. Methods and Protocols for Reliable Electrochemical Testing in Post-Li Batteries (Na, K, Mg, and Ca). *Chem. Mater.* **2019**, *31*, 8613−8628.
(67) Ciobanu, M.; Wilburn, J. P.; Lowy, D. A. Miniaturized Reference Electrodes. II. Use in Corrosive, Biological, and Organic Media. *Electroanalysis* **2004**, *16*, 1351−1358.
(68) Kobayashi, T.; Susa, K.; Taniguchi, S. P-T-X Phase Equilibrium Study of New Solid Solution Systems, Cd,-,M,S (M = Mg, Ca, Sr). *J. Solid State Chem.* **1980**, *33*, 203−207.
(69) Citrin, P. H.; Wertheim, G. K.; Baer, Y. Many-Body Processes in x-Ray Photoemission Line Shapes from Li, Na, Mg, and Al Metals. *Phys. Rev. B* **1977**, *16*, 4256−4282.
(70) van Attekum, P. M. T. M.; Trooster, J. M. The Resolution Obtainable in X-Ray Photoelectron Spectroscopy with Unmonochromatized Mg Kα Radiation. *J. Electron Spectrosc. Relat. Phenom.* **1980**, *18*, 135−143.

https://doi.org/10.1021/acsami.2c19488
ACS Appl. Mater. Interfaces XXXX, XXX, XXX−XXX